Research article

Influence of NiO into the CO_2 capture of Li_4SiO_4 and its catalytic performance on dry reforming of methane

Ariadna González [a], Miguel A. Martínez-Cruz [b], Brenda Alcántar-Vázquez [c], Nora S. Portillo-Vélez [d], Heriberto Pfeiffer [b], Hugo A. Lara-García [a],[*]

[a] *Instituto de Física, Universidad Nacional Autónoma de México, Apartado Postal 20364, CDMX, 01000, Mexico*
[b] *Instituto de Investigaciones en Materiales, Universidad Nacional Autónoma de México, Cd. Universitaria, Del. Coyoacán, CP 04510, CDMX, Mexico*
[c] *Instituto de Ingeniería, Universidad Nacional Autónoma de México, Avenida Universidad 3000, Coyoacán, CP 04510, CDMX, Mexico*
[d] *Depto. De Química, Área de Catálisis, Universidad Autónoma Metropolitana-Iztapalapa, Av. San Rafael Atlixco No. 189, Iztapalapa, CDMX, 09340, Mexico*

A B S T R A C T

Carbon capture, utilization, and storage (CCUS) technology offer promising solution to mitigate the threatening consequences of large-scale anthropogenic greenhouse gas emissions. Within this context, this report investigates the influence of NiO deposition on the Li_4SiO_4 surface during the CO_2 capture process and its catalytic behavior in hydrogen production via dry methane reforming. Results demonstrate that the NiO impregnation method modifies microstructural features of Li_4SiO_4, which positively impact the CO_2 capture properties of the material. In particular, the NiO–Li_4SiO_4 sample captured twice as much CO_2 as the pristine Li_4SiO_4 material, 6.8 and 3.4 mmol of CO_2 per gram of ceramic at 675 and 650 °C, respectively. Additionally, the catalytic results reveal that NiO–Li_4SiO_4 yields a substantial hydrogen production (up to 55 %) when tested in the dry methane reforming reaction. Importantly, this conversion remains stable after 2.5 h of reaction and is selective for hydrogen production. This study highlights the potential of Li_4SiO_4 both a support and a captor for a sorption-enhanced dry reforming of methane. To the best of our knowledge, this is the first report showcasing the effectiveness of Li_4SiO_4 as an active support for Ni-based catalysis in the dry reforming of methane. These findings provide valuable insights into the development of this composite as a dual-functional material for carbon dioxide capture and conversion.

1. Introduction

The fast increase in the world population has driving up energy requirements. As it is well known, fossil fuels represent the main energy source, and demand is expected to continue raising [1]. However, as long as they continue to be used, the anthropogenic emissions of greenhouse gases, mainly CO_2, are likely to continue increasing as well. This, in turn, exacerbates global warming and poses a threat to the climate [2]. In the context of strengthening the global response to the threat of climate change, the Intergovernmental Panel on Climate Change (IPCC) has assessed the impacts of global warming reaching 1.5 °C above pre-industrial levels and

---

the associated greenhouse gas emission pathways. If the 1.5 °C global warming target is achieved, adaptation will be less difficult, with fewer negative impacts on the intensity and frequency of extreme events, on resources, ecosystems, biodiversity, food security, cities, and tourism. The global response to warming of 1.5 °C comprises transitions and mitigation options in land and ecosystem, energy, urban and infrastructure, and industrial systems [3]. One option to mitigate a significant part of the impact of greenhouse gases before the necessary transformation of the energy supply is carbon capture, utilization, and storage (CCUS) technologies [4,5].

In this regard, solid sorbents possess potential advantages, including reduced energy requirements for CO_2 capture and a lack of liquid waste streams [6]. Among them, lithium ceramics are well-known for their good properties as high-temperature solid sorbents [6–8]. In fact, lithium orthosilicate (Li_4SiO_4) stands out due to its attractive features as CO_2 sorbent. The principal advantages of this material are high CO_2 capture capacity, low desorption temperature (<750 °C), excellent cycle stability, and better sorption kinetics compared with other alkaline ceramics [9–12]. In recent years, the scientific community has focused its attention on improving the CO_2 capture capacities of this kind of materials through various approaches: 1) using different synthesis methods [13,14], conventionally, lithium orthosilicate is synthesized through a solid-state reaction [15,16], but, alternative synthesis methods have been reported, including hydrothermal, plasma irradiation and sol-gel, among others [17–20]; 2) doping with different metals, such as germanium [21], iron [22], aluminum, vanadium [23], as well as potassium, magnesium, chromium and cerium [24]; 3) coating with different compounds, such as gluconic acid-based carbon [25] [] and K_2CO_3 ,[26,27] and, 4) modifying their microstructural features by a ball milling process after a solid-state synthesis [22,28]. All these modifications improve the CO_2 capture capacity of Li_4SiO_4. According to Equation (1), Li_4SiO_4 is able to trap up to 36.7 wt% or 8.34 mmol of CO_2 per gram of ceramic, and the experimental capture has achieved 95 % of its theoretical value, that is, 35 wt% [18].

$$Li_4SiO_4(s) + CO_2(g) \leftrightarrow Li_2SiO_3(s) + Li_2CO_3(s), \ \Delta H_{298K} = -143 \ kJ/mol \tag{1}$$
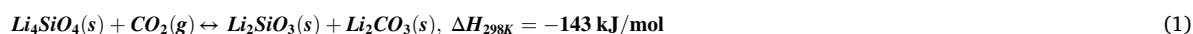
On the other hand, the dry reforming of methane (DRM) reaction, Equation (2), is a catalytic route suitable for the diminution of two abundant atmosphere pollutants, carbon dioxide and methane [29]. The reaction products, hydrogen and carbon monoxide (a mixture known as syngas), are the base for producing a great variety of high-value chemicals [30]. Nickel-based catalysts have been widely employed in the DRM reaction owing to their high activity, considerable availability and low cost [31–34].

$$CH_4 + CO_2 \rightarrow 2H_2 + 2CO, \ \Delta H_{298K} = 247 \ kJ/mol \tag{2}$$

Alkaline and alkaline earth metals are widely used as support or promoter because they play an important role in some reactions, such as DRM, by increasing the basicity of the catalyst. This accelerates the activation of acidic CO_2, which oxidizes the carbon on the surface. The presence of activated CO_2 on the catalyst surface inhibits the carbon formed by the CH_4 decomposition reaction, improving the resistance to deactivation [32,34,35].

Furthermore, with the aim of improving the traditional CCUS process and mitigating associated costs and energy consumption, a recent innovation known as integrated carbon capture and utilization (ICCU) has emerged. ICCU aims to capture CO_2 emissions and convert them directly into value-added chemical products or fuels using a blend of sorbent/catalyst materials or dual functional materials (DFM) [36,37]. These advantages not only make ICCU an environmentally friendly approach to carbon emissions reduction but also position it as a promising and cost-effective solution for industries seeking to mitigate their carbon footprint while simultaneously generating valuable chemical products and fuels.

Typically, the adsorptive element comprises alkali metal oxides or carbonates, offering basic sites for capturing CO_2 from exhaust gases in flue systems. Meanwhile, the catalytic component can efficiently transform the adsorbed CO_2 into diverse value-added products. Recently, sodium and lithium zirconates (Na_2ZrO_3, Li_2ZrO_3) [38], NiO–CaO composites [39], and Ni-doped Na_2ZrO_3 [40] have been tested as potential DFM that can act as sorbents and then as catalysts, allowing for consecutive CO_2 capture and DRM. These materials capture CO_2, store it, and supply it during the DRM process. Additionally, the sorption-enhanced process combines the H_2 production by steam methane reforming (SESMR) [41–43] or water gas shift (SEWGS) [44] or other catalytic reactions with an *in situ* CO_2 capture process. These processes have several advantages, including high-purity H_2 production, minimization of unfavourable side reactions, and reduced CO amounts in the gas effluent [37,38]. Different alkaline ceramics have been proposed as sorbents in these processes, including CaO [41,42], MgO [45], Li_2ZrO_3, Na_2ZrO_3, and Li_4SiO_4 [46]. In particular, Li_4SiO_4 has recently been studied as a sorbent in CO_2 methanation process (Li_4SiO_4@Ni/CeO_2) [47] and CH_4 reforming (Li_4SiO_4@Ni/Al_2O_3) [48], however, in both reports, another material was used to perform the reaction.

In this context, the aim of this study was to investigate the effect of adding NiO onto the Li_4SiO_4 surface on the carbon capture capacity of the composite. Additionally, the performance of NiO–Li_4SiO_4 as a catalyst for hydrogen production through dry reforming of methane and as a dual functional material was evaluated. This study represents the first report on the use of NiO–Li_4SiO_4 composite as both CO_2 capture material and catalyst for H_2 production via DRM reaction, providing valuable insights for future research in this field.

2. Experimental section

Lithium orthosilicate was synthesized by a solid-state reaction using silica (SiO_2, 99.9 % purity, Aldrich) and lithium oxide (Li_2O, 97 % purity, Aldrich) as reagents. To account for the possibility of lithium sublimation at high temperatures, an excess of 10 wt% of Li_2O was used [15]. The precursors were mechanically mixed and then heat-treated at 800 °C for 6 h. After the synthesis of Li_4SiO_4, nickel oxide (10 wt%) was deposited via wet impregnation using nickel nitrate (Ni(NO_3)$_2$·6H_2O, Aldrich) as a reagent. A different composition with 5 wt% of Ni was studied, however, its catalytic activity in the DRM was found to be poor (see Fig. S1). As a result, it

was decided not to include it in the main text. The appropriate amount of nickel nitrate was dissolved in 1 mL of deionized water and added dropwise to 1 g of Li$_4$SiO$_4$. The final powder was dried and heated at 600 °C for 6h. Hereinafter, this material is labelled NiO–Li$_4$SiO$_4$.

Li$_4$SiO$_4$ and NiO–Li$_4$SiO$_4$ samples were structurally and texturally characterized using powder X-ray diffraction (XRD), N$_2$ adsorption-desorption, and scanning electron microscopy (SEM). XRD patterns were recorded in the range of $15° \leq 2\Theta \leq 80°$, with a goniometer speed of $1.16°$ (2θ) min^{-1}, using a Siemens D5000 diffractometer equipped with a cobalt anode ($\lambda = 1.789$ Å) X-ray tube. Compounds were conventionally identified using the PDF database. Once the crystalline structures of Li$_4$SiO$_4$ and NiO–Li$_4$SiO$_4$ were determined, N$_2$ adsorption-desorption isotherms were measured at 77 K using a multipoint technique with a Minisorp II instrument from Bel-Japan. Prior to physisorption experiments, samples were degassed at room temperature for 12 h. The specific surface area of each material was calculated using the BET model. Parallelly, H$_2$ temperature programmed reduction (H$_2$-TPR) experiments were conducted using a Belcat B chemisorption analyzer from Bel Japan. For these measurements, samples were pre-treated at 800 °C in air flow (30 mL/min) and then cooled to 50 °C while flowing He to purge any products formed, such as water or carbon residues. Afterwards, 50 mg of the sample was reduced using H$_2$ (10 % of H$_2$, Ar balance (50 mL/min)) with a temperature ramp of 10 °C/min. Regarding the CO$_2$-TPD experiments, 50 mg of the sample was first treated in a He flow at 700 °C for 1 h to clean the surface, and then it was cooled to the adsorption temperature (100 °C) under He flow. Then, the materials were exposed to a flow of 5 % CO$_2$ mol fraction (50 mL/min, with He as a balance gas) for 60 min. The CO$_2$-TPD was performed by increasing the temperature to 750 °C, using a 10 °C/min ramp under a flow of He. Scanning electron microscopy (SEM) images were recorded using a JEOL JMS-7800F electron microscope equipped with an Oxford X-Max^{50} energy-dispersive analysis detector. Chemical superficial analysis was performed by X-ray photoelectron spectroscopy (XPS) in an ultra-high vacuum (UHV) system, the Scanning XPS microprobe PHI 5000 VersaProbe II. This instrument was equipped with a monochromatic X-ray source (h$\nu = 1486.6$ eV) with a 100 μm beam diameter and a MCD analyzer. The surface of samples was not etched. The XPS spectra were acquired at a 45° angle to the normal surface in the constant pass energy mode (CAE) with E$_0 = 117.40$ eV for survey scans and 11.75 eV for high-resolution narrow scans. Finally, The Raman experiments were conducted using the Horiba Xplora Plus Raman Microscope. A 532 nm laser was used, and a 50× objective was employed to focus the laser radiation on the sample. Each Raman measurement was carried out for a duration of 12 s, and 10 acquisitions were accumulated to enhance the data quality.

Carbon dioxide capture experiments were performed using a Q500HR thermobalance from TA Instruments. Li$_4$SiO$_4$ and NiO–Li$_4$SiO$_4$ samples were dynamically heat-treated from room temperature to 800 °C with a heating rate of 3 °C/min. Additionally, Li$_4$SiO$_4$ and NiO–Li$_4$SiO$_4$ samples were heat-treated isothermally at 550, 600, 650, and 675 °C. These experiments were performed using ~30 mg of sample and a carbon dioxide (CO$_2$, Praxair grade 3.0) flow rate of 60 mL/min (standard conditions).

The catalytic performance of Li$_4$SiO$_4$ and NiO–Li$_4$SiO$_4$ in the DRM reaction was evaluated using a Bel-Rea catalytic reactor from Bel-Japan with 200 mg of sample. The DRM process was performed with a temperature range from 200 to 900 °C at a heating rate of 2 °C/min. A mixture of a gas composed of 5 mL/min (standard conditions) of CH$_4$ (Praxair grade 5.0), 5 mL/min (standard conditions) of CO$_2$ (Praxair grade 3.0) and 50 mL (standard conditions) of N$_2$ (Praxair grade 4.8) as balance gas was used. Subsequently, isothermal experiments were carried out at 700, 725, 750, and 775 °C maintaining the same gas mixture ratio.

Additionally, DRM experiments were also performed with a previous CO$_2$ capture step. In this case, samples were previously carbonated at 675 °C for 3 h, using 60 mL/min (standard conditions) of CO$_2$. Then, the carbonated sample was heated to 750 °C, and the gas mixture was switched to the following composition: 5 mL/min of CH$_4$ and 55 mL/min of N$_2$ for 3 h. Finally, NiO–Li$_4$SiO$_4$ catalytic performance in methane decomposition reaction was studied dynamically from 200 to 900 °C using a gas composition of 5 mL/min (standard conditions) of CH$_4$ and 55 mL/min (standard conditions) of N$_2$. Catalytic gas products were analyzed every 15 °C up to 900 °C (dynamic experiments), or every 8.3 min (isothermal experiments), using a Shimadzu GC-2014 gas chromatograph with a Carbonex-1000 column coupled to a TCD detector. Calibration curves were used to quantify each gas product or reactant. The CH$_4$ conversion and H$_2$ and CO efficiency were calculated as follows, by equations (3)–(5):
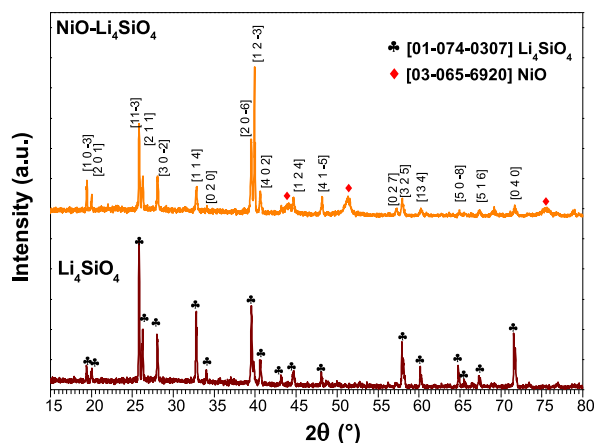
Fig. 1. XRD patterns of Li$_4$SiO$_4$ and NiO–Li$_4$SiO$_4$ samples.

$$\%CH_4 = \frac{[CH_4]_i}{[CH_4]_o} \, x100 \tag{3}$$

$$\%H_2 = \frac{[H_2]_i}{2[CH_4]_o} \, x100 \tag{4}$$

$$\%CO = \frac{[CO]_i}{2[CH_4]_o} \, x100 \tag{5}$$

Where $[CH_4]_i$, $[H_2]_i$, and $[CO]_i$ are the methane, hydrogen and carbon monoxide concentrations in each GC measurement, while $[CH_4]_o$ corresponds to the initial methane concentration. Afterwards isothermal CO_2 capture and DRM experiments, certain materials were re-characterized by XRD, Raman and SEM.

3. Results and discussion

Fig. 1 shows the XRD patterns of both samples. The diffraction peaks of Li_4SiO_4 were observed in the bare sample (PDF 01-074-0307 file), indicating that Li_4SiO_4 crystallizes in the monoclinic $P2_1/m$ space group. When nickel was loaded, the Li_4SiO_4 crystal structure was preserved, as evident in the XRD pattern. Nevertheless, the (1 2–3) reflection becomes the main peak of the Li_4SiO_4 phase, suggesting a crystal reorientation. Previous studies have shown that when Li_4SiO_4 comes into contact with water, it forms Si–OH and Li–OH groups on its surface [49]. When NiO is deposited by wet impregnation, water enters in contact with the Li_4SiO_4 surface, resulting in the formation of the OH groups. Subsequently, the composite was dried at 600 °C, inducing the Li_4SiO_4 recrystallization from Li–OH and Si–OH groups, as shown in the diffraction pattern of NiO–Li_4SiO_4 (Fig. 1). This process may be responsible for the crystal reorientation. It is important to note that the (1 2–3) plane is mainly composed of lithium atoms, as shown in Fig. S2. In addition, other reflections located at 43.8 and 50.9, on the 2θ scale were observed. These two diffraction peaks are associated to NiO (PDF 03-065-6920 file). Therefore, the Ni was impregnated over the Li_4SiO_4 surface as nickel oxide (NiO), forming a composite. The NiO crystallite size, estimated by the Scherrer equation, was 14.2 nm.

The materials were texturally characterized by N_2 adsorption-desorption (Fig. S3) and scanning electron microscopy (Fig. 2). Both materials exhibited isotherms type II without a hysteresis loop. According to the IUPAC classification, this type of isotherm is typically associated with non-porous or macroporous materials [50]. The specific surface areas were calculated using the BET model. The
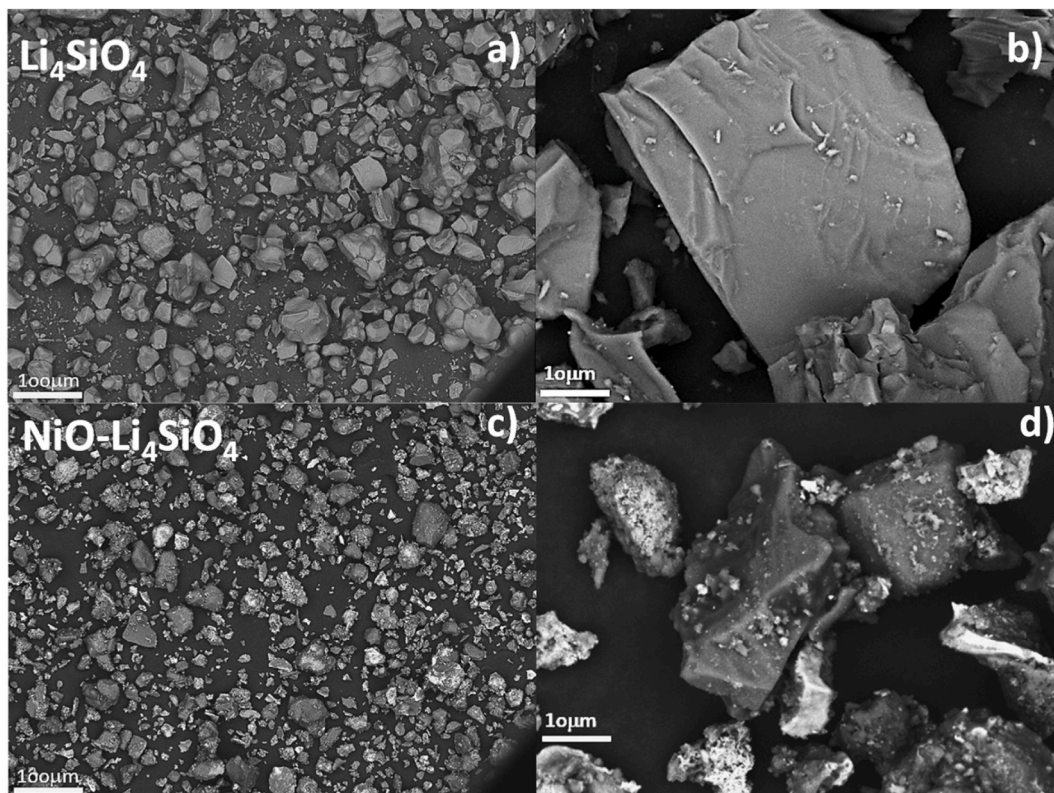
Fig. 2. SEM images obtained with backscattered electrons of Li_4SiO_4 (a and b) and NiO–Li_4SiO_4 (c and d) samples at two different magnifications.

pristine material has an area of 1 m^2/g while the $NiO–Li_4SiO_4$ presents an area of 2 m^2/g. Thus, the specific surface area doubles after the impregnation process. This increase can be attributed to the dispersion of Ni over the surface of the Li_4SiO_4, but it is primarily due to the reduction of the particle sizes, which will be discussed below. A similar result was found in a previous report; the textural properties of CaO, particularly the specific surface area, increase after a Ni wet impregnation method [51]. While the increase in specific surface area may seem insignificant, this modification enhances the number of basic sites and, therefore, has a positive impact on the capture properties, as will be demonstrated ahead.

Complementing the microstructural analysis, SEM images with backscattered electrons was conducted on both samples (Fig. 2). The Li_4SiO_4 sample (Fig. 2 a) and b)) displayed highly heterogeneous large particle with sizes ranging between 5 and 120 μm, while the $NiO–Li_4SiO_4$ sample exhibited particle sizes between 5 and 80 μm. These results are consistent with the increase in the surface area previously determined; the particle sizes are smaller in the composite than in the pristine Li_4SiO_4 material. Furthermore, the images of $NiO–Li_4SiO_4$ reveal two different phases characterized by differences in its mean atomic number ($\overline{Z}$). Li_4SiO_4 has a $\overline{Z}$ of 8.5, while NiO has a $\overline{Z}$ of 23.5. Consequently, the backscattered electron coefficient (η) [52] for these phases increases from 0.097 for Li_4SiO_4 (the dark phase) to 0.258 for NiO (the bright phase). Additionally, the distribution of NiO on the Li_4SiO_4 surface appears to be heterogeneous, and some agglomeration of Ni is evident, as can be seen in Fig. 2 (c and d), where several particles larger than (10 μm) are fully covered by NiO.

The reducibility properties of Li_4SiO_4, $NiO–Li_4SiO_4$, and NiO nanoparticles from Sigma-Aldrich, which were employed for comparison, were investigated through H_2-TPR experiments, as shown in Fig. 3. Li_4SiO_4 did not exhibit reduction peaks, indicating its stability under a hydrogen atmosphere within the tested temperature range. In contrast, three distinct reduction peaks were observed for $NiO–Li_4SiO_4$, occurring in the temperature range of 380–700 °C. It is well-established that the reducibility temperatures depend on the interaction between the metal and the support material. A strong interaction between metal and support results in higher reduction temperatures [53]. The reduction events below 400 °C can be attributed to free NiO species undergoing reduction to metallic Ni, with minimal or no interaction with the support, as evidenced by the reduction profile of bare NiO nanoparticles. When NiO is supported on Li_4SiO_4, the reduction peaks are shifted to higher temperatures, indicating a strong interaction with the support surface. The initial reduction peak occurs at approximately 380 °C, followed by a second peak at 450 °C. These two peaks correspond to the uptake of hydrogen by surface-bound nickel oxide species. Additionally, a minor β TPR peak centered around 565 °C corresponds to the reduction of Ni^{2+} species to metallic Ni with a stronger interaction with the alkaline support [32,54].

It is well known that basic sites play a fundamental role in methane dry reforming. These basic sites promote the activation of acidic CO_2 on the catalyst support's surface while preventing carbon deposition on the catalyst [55]. To discern the nature of these basic sites, CO_2-TPD experiments were conducted for both materials, as illustrated in Fig. 4. Li_4SiO_4 displays a desorption peak centered at 200 °C, while $NiO–Li_4SiO_4$ exhibits a peak at 190 °C. The temperature range of these peaks provides insights into the type of basic sites present. In both materials, weak Brønsted basic sites are identified, falling within the temperature range of 100–250 °C [55]. The main difference lies in the peak intensity, with the impregnation of NiO significantly increasing the number of basic sites. As demonstrated below, this increase positively impacts the material's capture capacities.

After the characterization process, the carbon dioxide capture properties of both samples were evaluated dynamically and isothermally in a thermobalance under a saturated atmosphere of CO_2. Fig. 5-a shows the dynamic TG graphs of both samples. In the Li_4SiO_4 sample, CO_2 chemisorption began at 450 °C, and the maximum capture was achieved at 645 °C (9.5 wt %). At higher temperatures, the desorption process is observed, which is in good agreement with previous reports on Li_4SiO_4 [9,10]. On the other hand, in the case of Ni-containing lithium orthosilicate, CO_2 capture is observed from 90 °C (Fig. 5-a inset). However, at temperatures lower than 480 °C, chemisorption is low, here, the superficial reaction is taking place. Usually, superficial and bulk CO_2 sorption processes are indistinguishable in lithium orthosilicate [19,28]. It is worth noting that in the pristine sample, superficial CO_2 chemisorption is not observed. The improvement in surface chemisorption on $NiO–Li_4SiO_4$ is related to the increased number of basic sites resulting
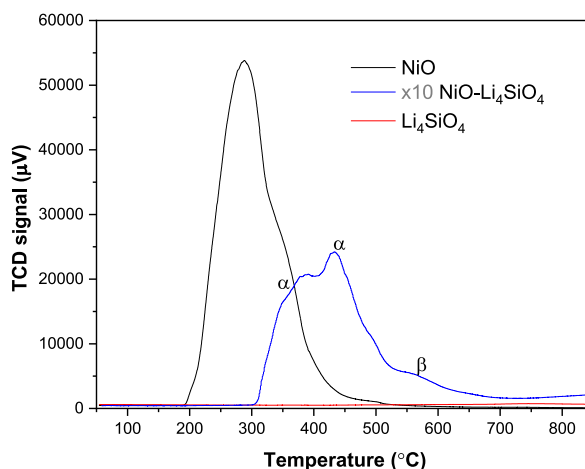
Fig. 3. TPR profiles of Li_4SiO_4 (red line), $NiO–Li_4SiO_4$ (blue line) and NiO nanoparticles (black line).
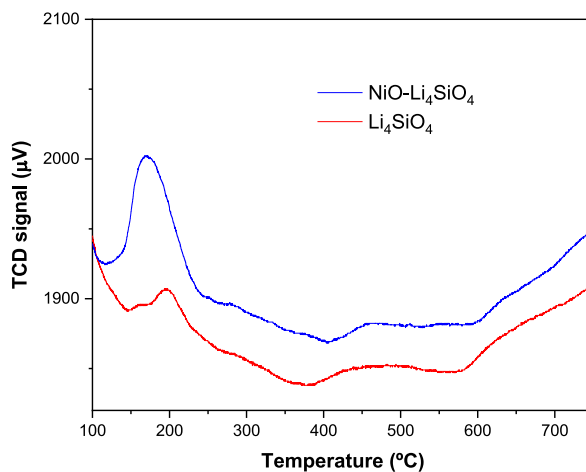
Fig. 4. TPD experiments of CO_2 adsorption at 100 °C of Li_4SiO_4 and NiO–Li_4SiO_4.
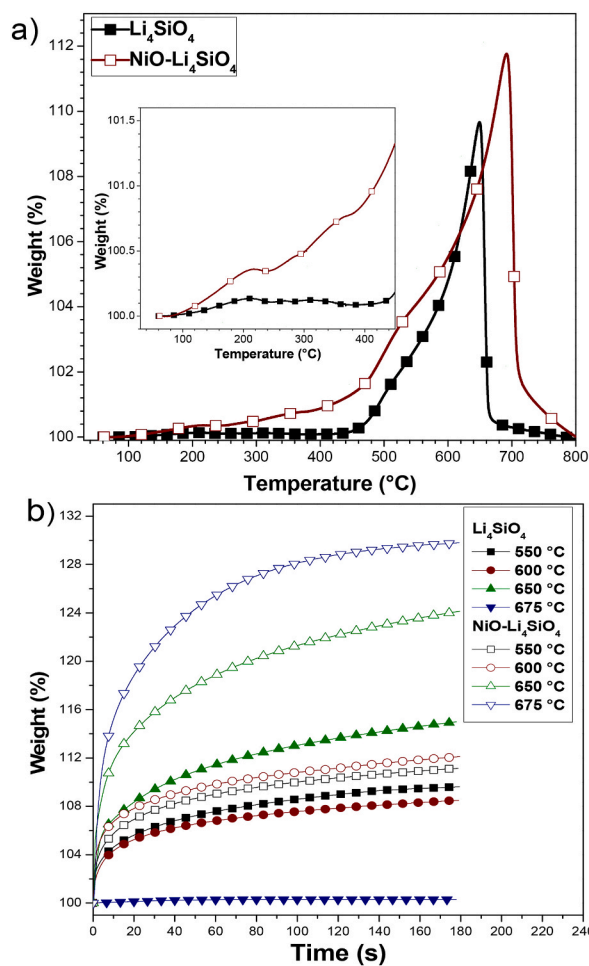
Fig. 5. a) Dynamic and b) isothermal thermogravimetric curves of Li_4SiO_4 and NiO–Li_4SiO_4 under a saturated atmosphere of CO_2.

from the addition of NiO, as demonstrated by CO_2-TPD experiments.

Afterwards, an abrupt increment is observed at 480 °C, resulting in CO_2 capture up to 11.8 wt % at 690 °C. This process take place in two different steps, the first one between 480 and 560 °C and the second between 560 and 690 °C. The first step is associated with the

finalization of the external shell formation. This external shell is composed of lithium carbonate (Li_2CO_3) and lithium metasilicate (Li_2SiO_3) (reaction 1). The second step is likely governed by the diffusion processes through this shell [19]. Another important change observed in the NiO-containing Li_4SiO_4 sample is that the desorption process was shifted to higher temperatures. In the pristine sample, it was observed at 650 °C, while in the Ni-containing sample, it started at around 690 °C. Therefore, the Ni addition improves CO_2 capture and extends the temperature range. It has been reported by previous studies [28] that even small increments in the specific surface area, such as in this case, enhance the CO_2 chemisorption in Li_4SiO_4, and the desorption process is shifted to higher temperatures.

Based on the previous TG dynamic results, CO_2 chemisorption was studied isothermally in both samples (Fig. 5-b). At 550 °C, CO_2 chemisorption on Li_4SiO_4 increases up to 9.5 wt %, then at 600 °C, the sorption decreases slightly to 8.5 wt %. Similar behavior has been previously observed in lithium-containing ceramics, which is related to a surface sintering process that occurs during the sample's heating [56,57]. The isotherm performed at 650 °C increased its final weight to 15 wt %, corresponding to 3.4 mmol of CO_2 per gram of ceramic. The increase in the capture after the sintering process has been related to two different effects: the formation of pores favoring the CO_2 diffusion through the external shell (Li_2CO_3 and Li_2SiO_3) and the fully activated ionic diffusion of Li and O [57]. Finally, at 675 °C, the Li_4SiO_4 sample did not present a weight increment during the 3 h, since the CO_2 desorption process occurs at this temperature, as already described in the dynamic TG curve.

On the contrary, in the isotherms performed over $NiO–Li_4SiO_4$, the CO_2 capture increased as a function of temperature, being the best capture equal to 30 wt % (6.8 mmol of CO_2 per gram of ceramic) at 675 °C, which is twice the CO_2 capture observed on Li_4SiO_4 at 650 °C. These results should be related to the increase in the number of basic surface sites, which leads to enhance the CO2 capture. In fact, CO_2 chemisorption was higher in all the isothermal experiments on the Ni-containing sample. Moreover, the desorption process was not observed at 675 °C on the $NiO–Li_4SiO_4$ sample, confirming that the CO_2 chemisorption properties are modified by the NiO deposition on the Li_4SiO_4 surface.

After the isothermal experiments, the corresponding solid products were characterized by XRD and SEM analysis. Fig. 6 a) shows the XRD patterns of the $NiO–Li_4SiO_4$ product obtained at 675 °C. As expected, the pattern exhibited the formation of lithium carbonate (Li_2CO_3) and lithium metasilicate (Li_2SiO_3). Additionally, NiO was identified, but no other nickel-containing phases were detected. This suggests that $NiO–Li_4SiO_4$ captures CO_2 through the mechanism reported in previous studies [9–11] (reaction 1). Regarding the textural characterization (Fig. 6 b), it is evident that the particles have agglomerated after capture, with several particles exceeding 100 μm in size. Additionally, their surface roughness increased due to the formation of a lithium carbonate layer. In the inset, it can be
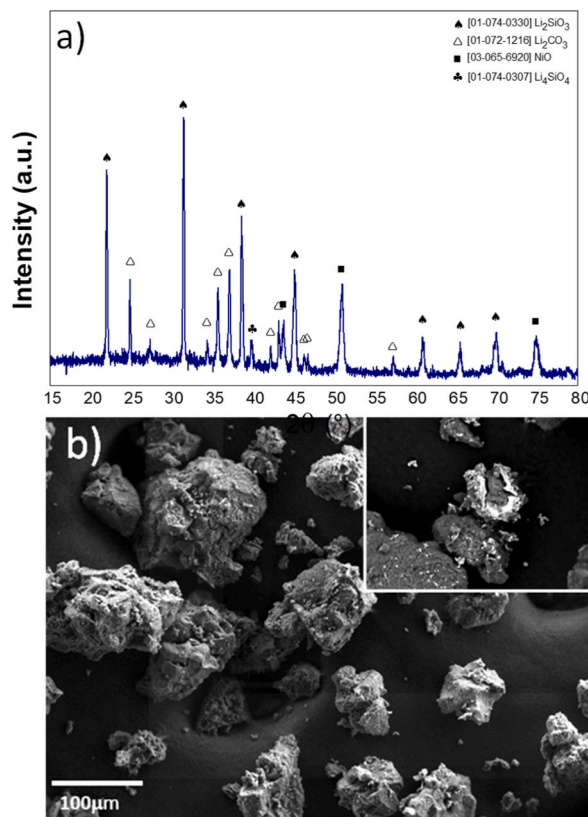
Fig. 6. a) XRD pattern and b) secondary and backscattered electron (inset) images of the $NiO–Li_4SiO_4$ isothermal product treated at 675 °C under a CO_2 saturated atmosphere.

noted that the dispersion of nickel remains heterogeneous, with some particles forming large clusters while others exhibit small particles.

After the CO_2 capture evaluation, the catalytic behavior in the DRM reaction process was studied. The DRM process was carried out from 200 to 900 °C, and the conversion and formation efficiencies were calculated using equations (3)–(5). When Li_4SiO_4 was tested (Fig. 7-a), only at high temperatures (>800 °C), some CH_4 conversion was observed (less than 5 %). However, no significant hydrogen production was observed, indicating that this material is practically inert for DRM reaction. On the contrary, the catalytic evolution of DRM over the NiO–Li_4SiO_4 sample showed a totally different behavior (Fig. 7-b). Hydrogen production was detected from 750 °C. At higher temperatures, H_2 formation increases exponentially as a function of the temperature, reaching a maximum efficiency of 75 % at 860 °C. At temperatures above 860 °C, hydrogen production remains stable. The H_2/CO ratio is lower than 1 at temperatures lower than 800 °C, indicating the occurrence of some no desirable reactions, such as the reverse water gas shift (RWGS). Between 650 and 1000 °C, RWGS is the main side reaction [33]. However, between 800 and 828 °C, the H_2/CO ratio was equal to 1, which means that parasitic reactions at these temperatures are no longer favored. Then, above 828 °C, the H_2/CO ratio was higher than 1, showing a good selectivity for hydrogen production.

As shown in Fig. 8, an isothermal experiment was carried out at 750 °C for 3 h to study the stability of the NiO–Li_4SiO_4 material. The gas mixture and catalyst amount were the same as in the dynamic experiment. It is evident that in the first 30 min, the catalytic conversion to hydrogen increases exponentially up to 42 %. Then, the efficiency rises slowly, reaching a maximum (55 %) after 80 min of reaction. After 3 h, the conversion tends to decrease up to 50 %. Therefore, it could be argued that H_2 production remains stable after 2 h of reaction. Additionally, the H_2/CO ratio was ≥1, indicating a high hydrogen selectivity and a decrease in unwanted reactions.

To determine the sample composition after the DRM process, the isothermal product was analyzed by XRD. As shown in Fig. 9-a, only Li_4SiO_4 and metallic Ni were identified, demonstrating that lithium silicate remains stable after the dry reforming process. However, the NiO was reduced to metallic Ni in the process as expected based on its reducibility properties. In this sense, it has been demonstrated that methane cracking can occur in the presence of some reducible metal oxides such as NiO. In these reducible oxides, lattice oxygen reacts with methane. Initially, CH_4 is partially oxidized by the lattice oxygen from the metal oxide, and the metal oxide is subsequently fully reduced to the metallic form [58,59]. Therefore, at the beginning of the reaction, hydrogen production comes from
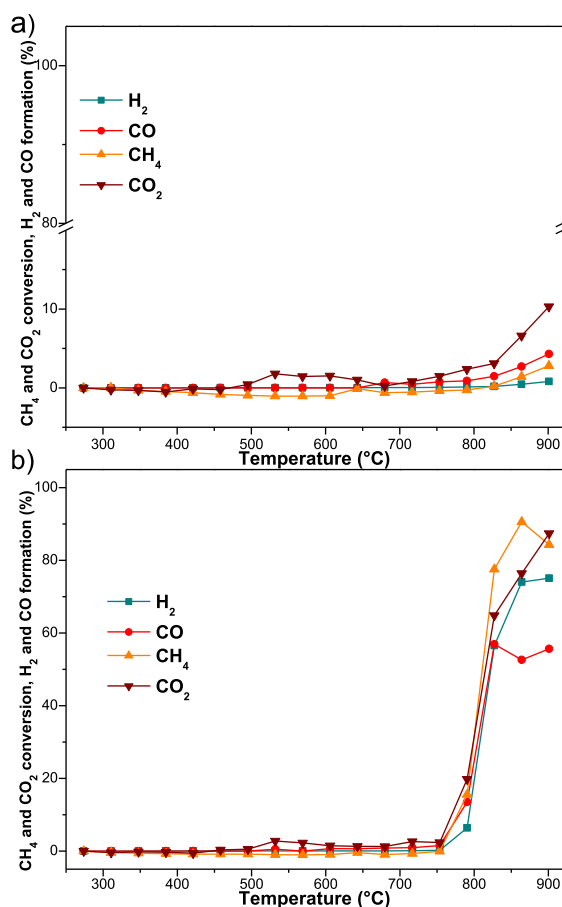
Fig. 7. Dynamic evolution for reactants (CO_2 and CH_4) and products (CO and H_2) obtained during the DRM using a) Li_4SiO_4 and b) NiO–Li_4SiO_4 as catalysts.
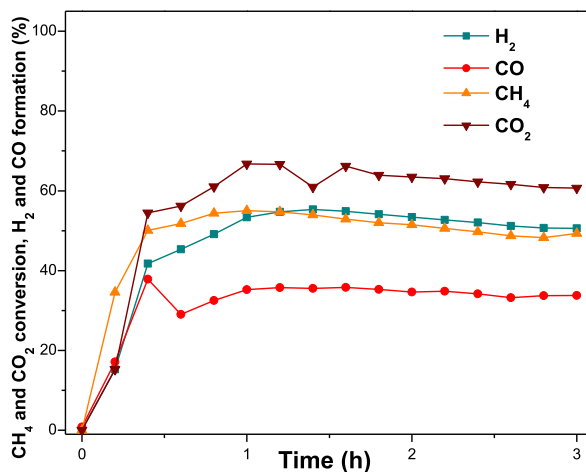
Fig. 8. Isothermal evolution of reactants (CO_2 and CH_4) and products (CO and H_2) at 750 °C, using NiO–Li_4SiO_4 as catalytic material.
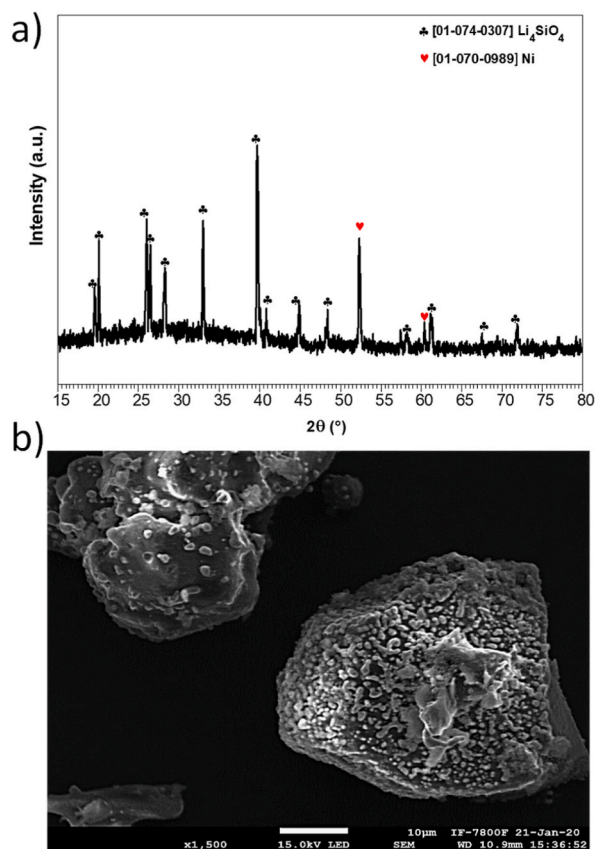
Fig. 9. a) XRD pattern and b) SEM image of the NiO–Li_4SiO_4 isothermal product of dry methane reforming performed at 750 °C.

methane decomposition. This chemical transformation should occur in the first 30 min of the reaction, during which the catalytic behavior is poor and increases as a function of the time. After this period, all NiO is reduced to Ni^0, and the conversion remains stable. The reduction of NiO was confirmed by XPS experiments. Fig. S4 shows the XPS spectra of the NiO–Li_4SiO_4 before (a) and after (b) the DRM experiment. It is evident that NiO was reduced to Ni^0 after the process. Furthermore, the microstructure of the isothermal product was analyzed through SEM analysis. As depicted in Fig. 9-b and Fig. S5, nickel (Ni) particles, ranging in size from 200 to 500 nm, are well dispersed across the surface of Li_4SiO_4. The observed changes in the sizes of the metallic Ni particles are attributed to the in-situ reduction of NiO. These particles are responsible to catalyze the DRM reaction.

It is worth noting that, despite its poor specific surface area (2 m^2/g) and relatively large nickel particle size, methane conversion is significantly high at 750 °C reaching 50 %. As mentioned previously, surface basic sites play a crucial role in the activation of CO_2 in the DRM process. Through CO_2-TPD experiments (as shown in Fig. 4), we confirmed the alkaline nature of Li_4SiO_4, and the introduction of NiO significantly enhances the abundance of basic sites on the catalyst's surface. As a result, CO_2 is adsorbed onto the Li_4SiO_4 surface via an acid-base interaction [60], facilitating the DRM catalytic process. DRM was also studied at different temperatures; Figs. S6 and S7 show the catalytic behavior at 725 and 775 °C, respectively. In both cases, a similar trend is observed: catalytic activity increases linearly during the first 30 min of the reaction, during which NiO is reduced to metallic Ni. The activity then remains stable for the next 150 min.

Finally, a two-step DRM process was studied. It has been demonstrated that some alkaline ceramics can serve as a dual functional material by using the CO_2 previously captured in the DRM reaction [38,40]. First, CO_2 was captured by NiO–Li_4SiO_4 at 675 °C for 1 h, after which the reactant gas was switched to CH_4, and the sample was heated to 750 °C to study the catalytic conversion of CH_4 with the previously trapped CO_2. It is important to note that these temperatures were chosen based on the CO_2 capture results and the lowest temperature at which the DRM was observed. Fig. 10 shows the evolution of the gases (CH_4, CO_2, H_2, and CO) as a function of time once the reactant gas was switched from CO_2 to CH_4. It is evident that the CO_2 amount decreases rapidly, and after 1 h, the CO_2 was no longer observed. This is because the CO_2 desorption process on the Ni-containing Li_4SiO_4 sample was observed at 690 °C (Fig. 5-a), and its availability is limited to the CO_2 previously captured. Therefore, when the gas is switched to CH_4, the CO_2 (previously adsorbed) begins to be desorbed from the lithium carbonate decomposition, and it is available as a reactant gas to perform the DRM reaction. In fact, the XRD pattern after the bifunctional process shows the presence of Li_4SiO_4, and no other Li and Si phases were observed, which means that the support is regenerated after the CO_2 desorption process (Fig. 11). Hydrogen production increased as a function of time from 9 % when the reaction started to 25 % when the CO_2 was completely consumed. In fact, it must be pointed out that there was a CH_4 conversion when CO_2 was no longer available, meaning hydrogen production should come from a methane decomposition reaction. After CO_2 consumption (~1 h), the hydrogen production starts to decrease linearly, reaching an efficiency of 17 % after 3 h of reaction. Furthermore, CO was barely observed in the first hour of reaction and was no longer observed after this time. A similar behavior was observed when Li_2ZrO_3 and Na_2ZrO_3 were tested as dual functional materials for hydrogen production through dry reforming of methane [38]; CO was almost negligible during all the reaction temperatures. This could be attributed to two different processes: coke deposition over the catalytic surface or hydrogen production from a methane decomposition reaction.

The presence of coke was confirmed by Raman experiments of the spent catalyst (Fig. S8). The two characteristics Raman bands of carbon were observed at 1340 cm^{-1} (D band) and 1550 cm^{-1} (G band). The D band indicates the presence of structural imperfections in the graphite layers, while the G band indicates the presence of in-plane or tangential mode stretching vibration of the sp^2 orbital atoms in the graphite layers. The intensity ratio of the D and G bands (ie, ID/IG values) was calculated to be 0.26. This value is less than one, suggesting a high degree of graphitization [61]. Therefore, the presence of coke deactivates the catalyst.

In order to demonstrate that methane decomposition is occurring, a dynamic methane decomposition experiment was performed from 200 to 900 °C, using the same amount of catalyst and only 5 mL/min of CH_4 (N_2 as gas balance). Fig. 12 shows the dynamic evolution of CH_4, H_2, CO_2, and CO from the catalytic decomposition of methane on NiO–Li_4SiO_4. Hydrogen production was detected from 500 °C, and its production remained around 5 % until 750 °C. After this temperature, H_2 formation increases as a function of the temperature, reaching a maximum value at 830 °C, where the efficiency was 29 %. Then, the conversion started to decrease, probably due to coke formation. Neither CO nor CO_2 was detected, meaning that carbon produced by the decomposition of methane was deposited over the catalyst surface, as in the previous case. This experiment, along with the lack of CO production, confirms that a methane decomposition reaction produces the hydrogen observed in the bifunctional process.

4. Conclusions and outlook

In summary, it has been demonstrated that the nickel impregnation method preserves the crystalline structure of Li_4SiO_4 but modifies its microstructural properties due to the hydroxylation process, which occurs when water reacts and alters the surface of lithium silicate. These microstructural changes increase the number of basic sites over the surface of Li_4SiO_4. These changes improve the CO_2 capture capacities in NiO–Li_4SiO_4, allowing it to trap twice the amount of CO_2 compared to the pristine sample. The catalytic results indicates that Li_4SiO_4 is an inert material for the dry reforming of methane reaction. However, when NiO was loaded onto lithium orthosilicate, the material was able to convert up to 55 % of methane into syngas. This conversion was demonstrated to be stable after 2.5 h of the reaction and highly selective for hydrogen. It should be noted that in the first 30 min of all the DRM tests, hydrogen production results in the reduction of NiO to metallic Ni. Once the Ni is reduced, the dry reforming reaction remains stable during the following 2.5 h of reaction. When NiO–Li_4SiO_4 was tested as a dual functional material, hydrogen production was observed, but it mainly results from methane decomposition. This effect arises from the fact that the dry reforming process occurs at higher temperatures than the CO_2 desorption process, with limited available CO_2. To enhance the overall efficiency of the two-step process, it is essential to shift dry reforming to lower temperatures. Achieving this goal requires better Ni dispersion, which can be accomplished by increasing the surface area of Li_4SiO_4.

This initial report presents promising results for employing NiO–Li_4SiO_4 composite as a sorbent and catalysts for catalytic hydrogen production, offering initial insights into its potential as a dual-functional material for a sorption-enhanced dry reforming of methane.

Data availability

Data associated with this study has not been deposited into a publicly available repository. Data will be made available on request.
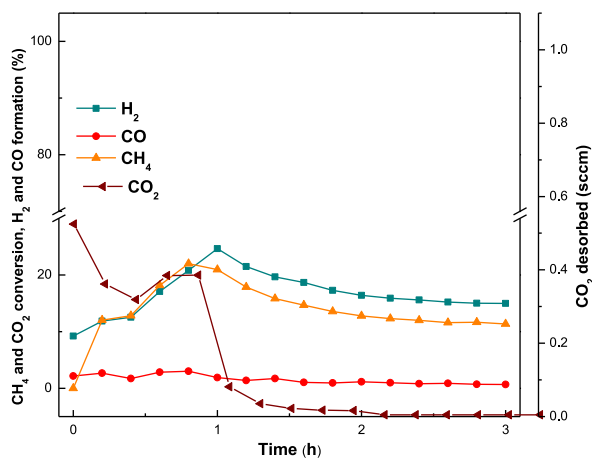
Fig. 10. Isothermal evolution of reactants (CO₂ and CH₄) and products (CO and H₂) obtained after a consecutive CO₂ capture at 675 °C and subsequent CH₄ dry reforming performed at 750 °C, using NiO–Li₄SiO₄ as active material.
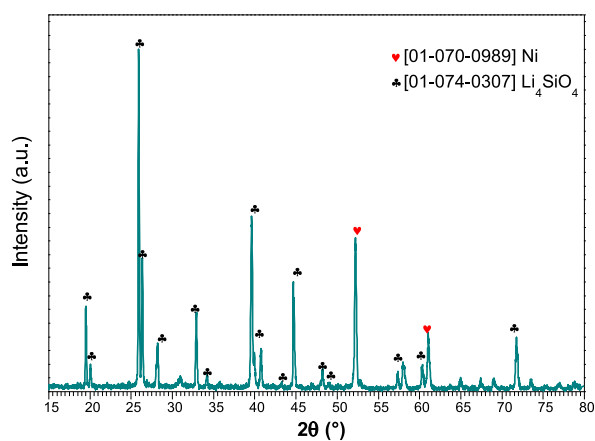
Fig. 11. XRD pattern of the NiO–Li₄SiO₄ isotherm product after a consecutive CO₂ capture and CH₄ dry reforming.
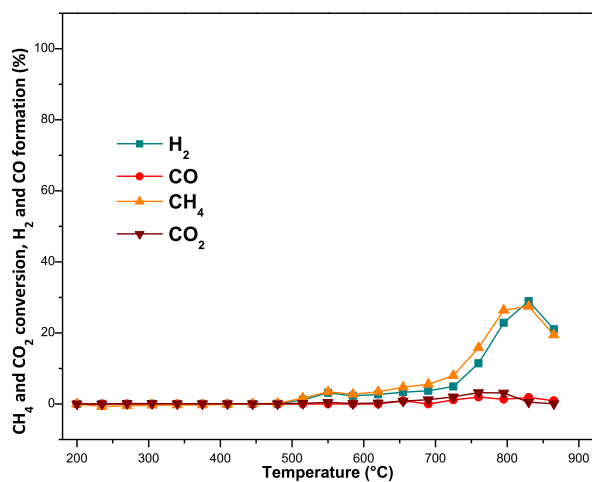
Fig. 12. Dynamic evolution (200–900 °C) for reactants (CO₂ and CH₄) and products (CO and H₂) obtained during the methane decomposition processes using NiO–Li₄SiO₄ as a catalyst.

CRediT authorship contribution statement

Ariadna González: Investigation, Formal analysis, Data curation. **Miguel A. Martínez-Cruz:** Methodology, Formal analysis, Data curation. **Brenda Alcántar-Vázquez:** Writing – review & editing, Investigation, Formal analysis. **Nora S. Portillo-Veléz:** Writing – review & editing, Investigation, Data curation. **Heriberto Pfeiffer:** Writing – review & editing, Methodology, Investigation, Funding acquisition. **Hugo A. Lara-García:** Writing – review & editing, Writing – original draft, Supervision, Project administration, Methodology, Conceptualization.

Declaration of competing interest

The authors declare that they have no known competing financial interests or personal relationships that could have appeared to influence the work reported in this paper.

Acknowledgements

Appendix A. Supplementary data

Supplementary data to this article can be found online at https://doi.org/10.1016/j.heliyon.2024.e24645.

References

[1] M. North, P. Styring, Perspectives and visions on CO_2 capture and utilisation, Faraday Discuss 183 (2015) 489–502, https://doi.org/10.1039/C5FD90077H.
[2] T.J. Crowley, Enhanced: CO_2 and climate change, Science 292 (80) (2001) 870–872, https://doi.org/10.1126/science.1061664.
[3] J.S. Masson-Delmotte, P. Zhai, H.-O. Pörtner, D. Roberts, E.L.P.R. Shukla, A. Pirani, W. Moufouma-Okia, C. Péan, R. Pidcock, S. Connors, J.B.R. Matthews, Y. Chen, X. Zhou, M.I. Gomis, T.W.T. Maycock, M. Tignor, Global warming of 1.5°C "An IPCC Special Report on the impacts of global warming of 1.5°C above pre-industrial levels and related global greenhouse gas emission pathways,", IPCC Spec. Rep. (630) (2018) 1.
[4] F. Nocito, A. Dibenedetto, Atmospheric CO_2 mitigation technologies: carbon capture utilization and storage, Curr. Opin. Green Sustainable Chem. 21 (2020) 34–43, https://doi.org/10.1016/j.cogsc.2019.10.002.
[5] F. Hussin, M.K. Aroua, Recent trends in the development of adsorption technologies for carbon dioxide capture: a brief literature and patent reviews (2014–2018), J. Clean. Prod. 253 (2020) 119707, https://doi.org/10.1016/j.jclepro.2019.119707.
[6] L. Bhatta, S. Seetharamu, S. Olivera, Lithium ceramics for high temperature CO_2 capture : a review, J. CPRI. 10 (2014) 395–408.
[7] Y. Zhang, Y. Gao, H. Pfeiffer, B. Louis, L. Sun, D. O'Hare, Q. Wang, Recent advances in lithium containing ceramic based sorbents for high-temperature CO_2 capture, J. Mater. Chem. A 7 (2019) 7962–8005, https://doi.org/10.1039/C8TA08932A.
[8] A. Yañez-Aulestia, H. Pfeiffer, The role of nickel addition on the CO_2 chemisorption enhancement in Ni-containing Li_2CuO_2: analysis of the cyclability and different CO_2 partial pressure performance, Fuel 277 (2020) 118185, https://doi.org/10.1016/j.fuel.2020.118185.
[9] X. Yan, Y. Li, X. Ma, J. Zhao, Z. Wang, Performance of Li_4SiO_4 material for CO_2 capture: a review, Int. J. Mol. Sci. 20 (2019) 928, https://doi.org/10.3390/ijms20040928.
[10] Y. Hu, W. Liu, Y. Yang, M. Qu, H. Li, CO_2 capture by Li_4SiO_4 sorbents and their applications: Current developments and new trends, Chem. Eng. J. 359 (2019) 604–625, https://doi.org/10.1016/j.cej.2018.11.128.
[11] S. Chen, J. Dai, C. Qin, W. Yuan, V. Manovic, Adsorption and desorption equilibrium of Li_4SiO_4-based sorbents for high-temperature CO_2 capture, Chem. Eng. J. 429 (2022) 132236, https://doi.org/10.1016/j.cej.2021.132236.
[12] L. Ma, C. Qin, S. Pi, H. Cui, Fabrication of efficient and stable Li_4SiO_4-based sorbent pellets via extrusion-spheronization for cyclic CO_2 capture, Chem. Eng. J. 379 (2020) 122385, https://doi.org/10.1016/j.cej.2019.122385.
[13] K. Wang, P. Zhao, X. Guo, Y. Li, D. Han, Y. Chao, Enhancement of reactivity in Li_4SiO_4-based sorbents from the nano-sized rice husk ash for high-temperature CO_2 capture, Energy Convers. Manag. 81 (2014) 447–454, https://doi.org/10.1016/j.enconman.2014.02.054.
[14] Y. Hu, M. Qu, H. Li, Y. Yang, J. Yang, W. Qu, W. Liu, Porous extruded-spheronized Li_4SiO_4 pellets for cyclic CO_2 capture, Fuel 236 (2019) 1043–1049, https://doi.org/10.1016/j.fuel.2018.09.072.
[15] M.J. Venegas, E. Fregoso-Israel, R. Escamilla, H. Pfeiffer, Kinetic and reaction mechanism of CO_2 sorption on Li_4SiO_4: study of the particle size effect, Ind. Eng. Chem. Res. 46 (2007) 2407–2412, https://doi.org/10.1021/ie061259e.
[16] M.T. Izquierdo, A. Turan, S. García, M.M. Maroto-Valer, Optimization of Li_4SiO_4 synthesis conditions by a solid state method for maximum CO_2 capture at high temperature, J. Mater. Chem. A 6 (2018) 3249–3257, https://doi.org/10.1039/c7ta08738a.
[17] X. Yang, W. Liu, J. Sun, Y. Hu, W. Wang, H. Chen, Y. Zhang, X. Li, M. Xu, Preparation of novel Li_4SiO_4 sorbents with Superior performance at low CO_2 concentration, ChemSusChem 9 (2016) 1607–1613, https://doi.org/10.1002/cssc.201501699.
[18] A. Nambo, J. He, T.Q. Nguyen, V. Atla, T. Druffel, M. Sunkara, Ultrafast carbon dioxide sorption kinetics using lithium silicate nanowires, Nano Lett. 17 (2017) 3327–3333, https://doi.org/10.1021/acs.nanolett.6b04013.
[19] P.V. Subha, B.N. Nair, P. Hareesh, A.P. Mohamed, T. Yamaguchi, K.G.K. Warrier, U.S. Hareesh, Enhanced CO_2 absorption kinetics in lithium silicate platelets synthesized by a sol–gel approach, J. Mater. Chem. A 2 (2014) 12792, https://doi.org/10.1039/C4TA01976H.
[20] P.V. Subha, B.N. Nair, V. Visakh, R. Achu, S. Shikhila, A. Peer Mohamed, T. Yamaguchi, U.S. Hareesh, Wet chemically derived Li_4SiO_4 nanowires as efficient CO_2 sorbents at intermediate temperatures, Chem. Eng. J. 406 (2021) 126731, https://doi.org/10.1016/j.cej.2020.126731.
[21] P.V. Subha, B.N. Nair, V. Visakh, C.R. Sreerenjini, A.P. Mohamed, K.G.K. Warrier, T. Yamaguchi, U.S. Hareesh, Germanium-incorporated lithium silicate composites as highly efficient low-temperature sorbents for CO_2 capture, J. Mater. Chem. A 6 (2018) 7913–7921, https://doi.org/10.1039/C8TA00576A.
[22] H.A. Lara-García, O. Ovalle-Encinia, J. Ortiz-Landeros, E. Lima, H. Pfeiffer, Synthesis of $Li_{4+x}Si_{1-x}Fe_xO_4$ solid solution by dry ball milling and its highly efficient CO_2 chemisorption in a wide temperature range and low CO_2 concentrations, J. Mater. Chem. A 7 (2019) 4153–4164, https://doi.org/10.1039/C8TA12359D.
[23] J. Ortiz-Landeros, I.C. Romero-Ibarra, C. Gómez-Yáñez, E. Lima, H. Pfeiffer, $Li_{4+x}(Si_{1-x}Al_x)O_4$ solid solution mechanosynthesis and kinetic analysis of the CO_2 chemisorption process, J. Phys. Chem. C 117 (2013) 6303–6311, https://doi.org/10.1021/jp4006982.

[24] K. Wang, Z. Yin, P. Zhao, Z. Zhou, Z. Su, J. Sun, Development of metallic element-stabilized Li$_4$SiO$_4$ sorbents for cyclic CO$_2$ capture, Int. J. Hydrogen Energy 42 (2017) 4224–4232, https://doi.org/10.1016/j.ijhydene.2016.10.058.

[25] K. Wang, Z. Zhou, P. Zhao, Z. Yin, Z. Su, J. Sun, Synthesis of a highly efficient Li$_4$SiO$_4$ ceramic modified with a gluconic acid-based carbon coating for high-temperature CO$_2$ capture, Appl. Energy 183 (2016) 1418–1427, https://doi.org/10.1016/j.apenergy.2016.09.105.

[26] Z. Zhou, K. Wang, Z. Yin, P. Zhao, Z. Su, J. Sun, Molten K$_2$CO$_3$-promoted high-performance Li$_4$SiO$_4$ sorbents at low CO$_2$ concentrations, Thermochim. Acta 655 (2017) 284–291, https://doi.org/10.1016/j.tca.2017.07.014.

[27] T. Zhang, M. Li, P. Ning, Q. Jia, Q. Wang, J. Wang, K$_2$CO$_3$ promoted novel Li$_4$SiO$_4$-based sorbents from sepiolite with high CO$_2$ capture capacity under different CO$_2$ partial pressures, Chem. Eng. J. 380 (2020) 122515, https://doi.org/10.1016/j.cej.2019.122515.

[28] I.C. Romero-Ibarra, J. Ortiz-Landeros, H. Pfeiffer, Microstructural and CO$_2$ chemisorption analyses of Li$_4$SiO$_4$: effect of surface modification by the ball milling process, Thermochim. Acta 567 (2013) 118–124, https://doi.org/10.1016/j.tca.2012.11.018.

[29] A. Movasati, S.M. Alavi, G. Mazloom, Dry reforming of methane over CeO$_2$-ZnAl$_2$O$_4$ supported Ni and Ni-Co nano-catalysts, Fuel 236 (2019) 1254–1262, https://doi.org/10.1016/j.fuel.2018.09.069.

[30] A. Abdulrasheed, A.A. Jalil, Y. Gambo, M. Ibrahim, H.U. Hambali, M.Y. Shahul Hamid, A review on catalyst development for dry reforming of methane to syngas: recent advances, Renew. Sustain. Energy Rev. 108 (2019) 175–193, https://doi.org/10.1016/j.rser.2019.03.054.

[31] G. Zhang, J. Liu, Y. Xu, Y. Sun, A review of CH$_4$–CO$_2$ reforming to synthesis gas over Ni-based catalysts in recent years (2010–2017), Int. J. Hydrogen Energy 43 (2018) 15030–15054, https://doi.org/10.1016/j.ijhydene.2018.06.091.

[32] W.J. Jang, J.O. Shim, H.M. Kim, S.Y. Yoo, H.S. Roh, A review on dry reforming of methane in aspect of catalytic properties, Catal. Today 324 (2019) 15–26, https://doi.org/10.1016/j.cattod.2018.07.032.

[33] H.A. Lara-García, D.G. Araiza, M. Méndez-Galván, S. Tehuacanero-Cuapa, A. Gómez-Cortés, G. Díaz, Dry reforming of methane over nickel supported on Nd-ceria: enhancement of the catalytic properties and coke resistance, RSC Adv. 10 (2020) 33059–33070, https://doi.org/10.1039/d0ra05761d.

[34] D. Wang, P. Littlewood, T.J. Marks, P.C. Stair, E. Weitz, Coking can enhance product yields in the dry reforming of methane, ACS Catal. 12 (2022) 8352–8362, https://doi.org/10.1021/acscatal.2c02045.

[35] S. Arora, R. Prasad, An overview on dry reforming of methane: strategies to reduce carbonaceous deactivation of catalysts, RSC Adv. 6 (2016) 108668–108688, https://doi.org/10.1039/c6ra20450c.

[36] Z. Lv, J. Ruan, W. Tu, X. Hu, D. He, X. Huang, C. Qin, Integrated CO$_2$ capture and In-Situ methanation by efficient dual functional Li$_4$SiO$_4$@Ni/CeO$_2$, Sep. Purif. Technol. 309 (2023) 123044, https://doi.org/10.1016/j.seppur.2022.123044.

[37] B. Shao, Y. Zhang, Z. Sun, J. Li, Z. Gao, Z. Xie, J. Hu, H. Liu, CO$_2$ capture and in-situ conversion: recent progresses and perspectives, Green Chem. Eng. 3 (2022) 189–198, https://doi.org/10.1016/j.gce.2021.11.009.

[38] J.A. Mendoza-Nieto, Y. Duan, H. Pfeiffer, Alkaline zirconates as effective materials for hydrogen production through consecutive carbon dioxide capture and conversion in methane dry reforming, Appl. Catal. B Environ. 238 (2018) 576–585, https://doi.org/10.1016/j.apcatb.2018.07.065.

[39] A. Cruz-Hernández, J.A. Mendoza-Nieto, H. Pfeiffer, NiO CaO materials as promising catalysts for hydrogen production through carbon dioxide capture and subsequent dry methane reforming, J. Energy Chem. 26 (2017) 942–947, https://doi.org/10.1016/j.jechem.2017.07.002.

[40] J.A. Mendoza-Nieto, S. Tehuacanero-Cuapa, J. Arenas-Alatorre, H. Pfeiffer, Nickel-doped sodium zirconate catalysts for carbon dioxide storage and hydrogen production through dry methane reforming process, Appl. Catal. B Environ. 224 (2018) 80–87, https://doi.org/10.1016/j.apcatb.2017.10.050.

[41] A. Di Giuliano, F. Giancaterino, C. Courson, P.U. Foscolo, K. Gallucci, Development of a Ni-CaO-mayenite combined sorbent-catalyst material for multicycle sorption enhanced steam methane reforming, Fuel 234 (2018) 687–699, https://doi.org/10.1016/j.fuel.2018.07.071.

[42] A. Di Giuliano, K. Gallucci, S.S. Kazi, F. Giancaterino, A. Di Carlo, C. Courson, J. Meyer, L. Di Felice, Development of Ni- and CaO-based mono- and bi-functional catalyst and sorbent materials for Sorption Enhanced Steam Methane Reforming: performance over 200 cycles and attrition tests, Fuel Process. Technol. 195 (2019) 106160, https://doi.org/10.1016/j.fuproc.2019.106160.

[43] A. Di Giuliano, F. Giancaterino, K. Gallucci, P.U. Foscolo, C. Courson, Catalytic and sorbent materials based on mayenite for sorption enhanced steam methane reforming with different packed-bed configurations, Int. J. Hydrogen Energy 43 (2018) 21279–21289, https://doi.org/10.1016/j.ijhydene.2018.10.003.

[44] R.W. Stevens, A. Shamsi, S. Carpenter, R. Siriwardane, Sorption-enhanced water gas shift reaction by sodium-promoted calcium oxides, Fuel 89 (2010) 1280–1286, https://doi.org/10.1016/j.fuel.2009.11.035.

[45] D.Y. Aceves Olivas, M.R. Baray Guerrero, M.A. Escobedo Bretado, M. Marques Da Silva Paula, J. Salinas Gutiérrez, V. Guzmán Velderrain, A. López Ortiz, V. Collins-Martínez, Enhanced ethanol steam reforming by CO$_2$ absorption using CaO, CaO*MgO or Na$_2$ZrO$_3$, Int. J. Hydrogen Energy 39 (2014) 16595–16607, https://doi.org/10.1016/j.ijhydene.2014.04.156.

[46] E. Ochoa-Fernández, T. Zhao, M. Rønning, D. Chen, Effects of steam addition on the properties of high temperature ceramic CO$_2$ acceptors, J. Environ. Eng. 135 (2009) 397–403, https://doi.org/10.1061/(asce)ee.1943-7870.0000006.

[47] Z. Lv, J. Ruan, W. Tu, X. Hu, D. He, X. Huang, C. Qin, Integrated CO$_2$ capture and In-Situ methanation by efficient dual functional Li$_4$SiO$_4$@Ni/CeO$_2$, Sep. Purif. Technol. 309 (2023) 123044, https://doi.org/10.1016/j.seppur.2022.123044.

[48] Z. Lv, C. Qin, S. Chen, D.P. Hanak, C. Wu, Efficient-and-stable CH$_4$ reforming with integrated CO$_2$ capture and utilization using Li$_4$SiO$_4$ sorbent, Sep. Purif. Technol. 277 (2021) 119476, https://doi.org/10.1016/j.seppur.2021.119476.

[49] J. Ortiz-Landeros, L. Martínez-dlCruz, C. Gómez-Yáñez, H. Pfeiffer, Towards understanding the thermoanalysis of water sorption on lithium orthosilicate (Li$_4$SiO$_4$), Thermochim. Acta 515 (2011) 73–78, https://doi.org/10.1016/j.tca.2010.12.025.

[50] M. Thommes, K. Kaneko, A.V. Neimark, J.P. Olivier, F. Rodriguez-Reinoso, J. Rouquerol, K.S.W. Sing, Physisorption of gases, with special reference to the evaluation of surface area and pore size distribution (IUPAC Technical Report), Pure Appl. Chem. 87 (2015) 1051–1069, https://doi.org/10.1515/pac-2014-1117.

[51] A. Di Giuliano, K. Gallucci, A. Di Carlo, S. Stendardo, C. Courson, P.U. Foscolo, Sorption enhanced steam methane reforming by Ni/CaO/mayenite combined systems: overview of experimental results from European research project ASCENT, Can. J. Chem. Eng. 98 (2020) 1907–1923, https://doi.org/10.1002/cjce.23779.

[52] H. Pfeiffer, K.M. Knowles, Reaction mechanisms and kinetics of the synthesis and decomposition of lithium metazirconate through solid-state reaction, J. Eur. Ceram. Soc. 24 (2004) 2433–2443, https://doi.org/10.1016/S0955-2219(03)00630-7.

[53] S. Das, S. Thakur, A. Bag, M.S. Gupta, P. Mondal, A. Bordoloi, Support interaction of Ni nanocluster based catalysts applied in CO$_2$ reforming, J. Catal. 330 (2015) 46–60, https://doi.org/10.1016/j.jcat.2015.06.010.

[54] Z. Bian, W. Zhong, Y. Yu, Z. Wang, B. Jiang, S. Kawi, Dry reforming of methane on Ni/mesoporous-Al$_2$O$_3$ catalysts: effect of calcination temperature, Int. J. Hydrogen Energy 46 (2021) 31041–31053, https://doi.org/10.1016/j.ijhydene.2020.12.064.

[55] M.A.A. Aziz, A.A. Jalil, S. Wongsakulphasatch, D.V.N. Vo, Understanding the role of surface basic sites of catalysts in CO$_2$ activation in dry reforming of methane: a short review, Catal. Sci. Technol. 10 (2020) 35–45, https://doi.org/10.1039/c9cy01519a.

[56] R. Rodríguez-Mosqueda, H. Pfeiffer, Thermokinetic analysis of the CO$_2$ chemisorption on Li$_4$SiO$_4$ by using different gas flow rates and particle sizes, J. Phys. Chem. A 114 (2010) 4535–4541, https://doi.org/10.1021/jp911491t.

[57] L. Martínez-Dlcruz, H. Pfeiffer, Microstructural thermal evolution of the Na$_2$CO$_3$ phase produced during a Na$_2$ZrO$_3$-CO$_2$ chemisorption process, J. Phys. Chem. C 116 (2012) 9675–9680, https://doi.org/10.1021/jp301917a.

[58] J. Adanez, A. Abad, F. Garcia-Labiano, P. Gayan, L.F. De Diego, Progress in chemical-looping combustion and reforming technologies, Prog. Energy Combust. Sci. 38 (2012) 215–282, https://doi.org/10.1016/j.pecs.2011.09.001.

[59] H.S. Lim, D. Kang, J.W. Lee, Phase transition of Fe_2O_3–NiO to $NiFe_2O_4$ in perovskite catalytic particles for enhanced methane chemical looping reforming-decomposition with CO_2 conversion, Appl. Catal. B Environ. 202 (2017) 175–183, https://doi.org/10.1016/j.apcatb.2016.09.020.

[60] A. Yañez-Aulestia, J.F. Gómez-García, J.A. Mendoza-Nieto, Y. Duan, H. Pfeiffer, Thermocatalytic analysis of CO_2-CO selective chemisorption mechanism on lithium cuprate (Li_2CuO_2) and oxygen addition effect, Thermochim. Acta 660 (2018) 144–151, https://doi.org/10.1016/j.tca.2017.12.027.

[61] M. Pudukudy, Z. Yaakob, Q. Jia, M.S. Takriff, Catalytic decomposition of methane over rare earth metal (Ce and La) oxides supported iron catalysts, Appl. Surf. Sci. 467 (468) (2019) 236–248, https://doi.org/10.1016/j.apsusc.2018.10.122.